
Locking Machine Learning Models into Hardware

Eleanor Clifford*, Cheng Zhang,
Yiren Zhao
Imperial College London

Adhithya Saravanan*, Harry Langford*,
Robert Mullins
University of Cambridge

Ilia Shumailov, Jamie Hayes
Google DeepMind

Abstract

Modern Machine Learning models are expensive IP and business competitiveness often depends on keeping this IP confidential. This in turn restricts how these models are deployed – for example it is unclear how to deploy a model on-device without inevitably leaking the underlying model. At the same time, confidential computing technologies such as Multi-Party Computation or Homomorphic encryption remain impractical for wide adoption. In this paper we take a different approach and investigate feasibility of ML-specific mechanisms that deter unauthorised model use by restricting the model to only be usable on specific hardware, making adoption on unauthorised hardware inconvenient. That way, even if IP is compromised, it cannot be trivially used without specialised hardware or major model adjustment. In a sense, we seek to enable cheap *locking of machine learning models into specific hardware*. We demonstrate that *locking* mechanisms are feasible by either targeting efficiency of model representations, such making models incompatible with quantisation, or tie the model’s operation on specific characteristics of hardware, such as number of cycles for arithmetic operations. We demonstrate that locking comes with negligible work and latency overheads, while significantly restricting usability of the resultant model on unauthorised hardware.

1 Introduction

The monetary expenditures associated with developing Machine Learning (ML) models are increasing rapidly with the advent of large generative models. Models with over a trillion parameters are now being trained on web-scale data [Brown et al., 2020]. These models have become valuable Intellectual Property (IP) assets, yet ensuring their competitive edge remains uncompromised when deployed on-device proves challenging. Competitors may reverse engineer the model’s architecture and parameters, redeploying it on their software and hardware stack. Concurrently, *governance* of Machine Learning models is a concern [Hadfield and Clark, 2023]. Especially in safety-critical applications, it may be necessary to limit model execution to special authenticated settings. Here, we usually rely on hardware and software combinations to prevent model use on unverified platforms which may lead to the potential misuse of the model.

Existing ML governance and IP protection methods can be classified into two categories: namely *policies* and *centralised serving*. Policy-based methods focus on either access control or licensing. For example, accessing Llama models requires users to sign a terms of service agreement [Touvron et al., 2023], and licenses like OpenRail [Ferrandis, 2022] include usage limitations to prevent misuse of these large language models (LLMs). However, it is entirely possible for these access-controlled models to leak, as it happened to LLama2 [Vincent, 2023], and malicious users may not adhere to any

*Shared first authorship

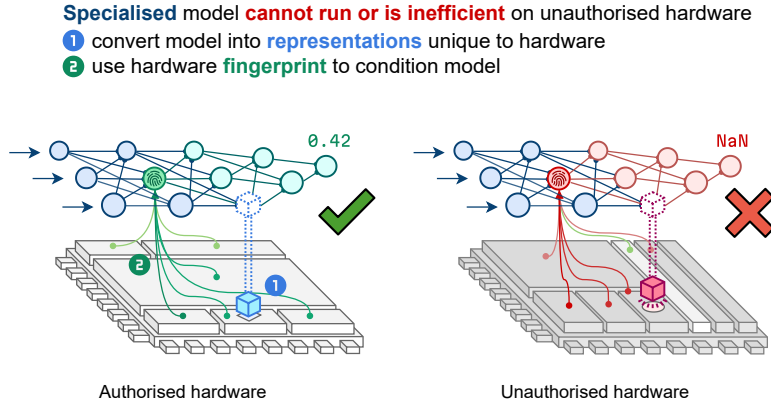


Figure 1: A high-level illustration of how *Machine Learning Locking* functions work is as follows: the locked model resists efficient, or any, deployment by adversaries on unauthorised hardware stacks. This resistance occurs because unauthorised hardware devices inherently lack support for some hardware operation or are unable to match the hardware properties of the authorised hardware.

existing licenses, as pointed out by Henderson et al. and Lin et al.. Another approach involves hosting ML models on centralised servers and providing standard API access to users. Companies employ this method to safeguard their IP, implementing safety filters and safeguarding prompts to ensure appropriate usage. It is worth mentioning that this centralised model serving necessitates substantial resources to maintain, as all user queries are handled by centralised computing infrastructure, unlike computations on user devices, which are typically less checked. Furthermore, these models cannot be used offline.

As both policy enforcement and centralised serving fail to address the issue of deploying whole or parts of ML models on user devices, we adopt a completely different approach from the aforementioned methods in this study, illustrated in Figure 1. We explore the feasibility of mechanisms enabling *Machine Learning Locking*, whereby a locked ML model resists efficient, or any, deployment by adversaries on unauthorised hardware stacks. In such scenarios, should a model be stolen or reverse-engineered, deploying it on unauthorised platforms would be either impossible or extremely challenging.

- We introduce the concept of *machine learning locking*, where ML models are locked to specific hardware stacks, restricting model usage on unauthenticated hardware.
- We demonstrate the feasibility of a range of software and hardware locking mechanisms; these methods have negligible overheads when deployed and we quantify the difficulty of breaking these locks on unauthorised hardware platforms.
- To the best of our knowledge, ours is the first work to explore hardware asymmetries as a foundation for governance and to discuss its implications for AI governance.

Table 1: Taxonomy of locking methods. For reverse engineering, access is given to the locked model but not the target hardware. * Similar to the cost of fine-tuning the model. ** The PUF method provides sufficient entropy to use the cheaper *AES encryption* transformation.

Category	Method	Effect	Reverse-engineering cost	Overhead
Soft locking	Sparsity-aware	Slowdown or Accuracy drop	Moderate*	Small
	Quantisation-aware	Slowdown or Accuracy drop	Moderate*	Small
Hard locking	Clock fingerprint	Accuracy drop	High	Moderate
	Finite Precision	Accuracy drop	High	Moderate
	SRAM PUF	Accuracy drop	Infeasible	Small**

Table 2: A comparison of the supported features of existing AI accelerators. * We consider also the TensorCore supported instruction for NVIDIA GPUs. TEE stands for the Trusted Execution Environment. ** DOJO utilised a specialised floating point arithmetic (CFP), where they have a different setup for exponent and mantissa bit widths.

Device		INT4	INT8	FP8	FP16	FP32	TF32	BFLOAT16	Sparsity	TEE
NVIDIA A100 *	Choquette et al. [2021]	✓	✓	✗	✓	✓	✓	✓	✓	✗
NVIDIA H100 *	Choquette [2023]	✗	✓	✓	✓	✓	✓	✓	✓	✓
NVIDIA H200 *	NVIDIA	✗	✓	✓	✓	✓	✓	✓	✓	✓
Cerebras WSE 2	Selig [2022]	✗	✗	✗	✓	✓	✗	✓	✓	✗
Tesla DOJO	Talpes et al. [2022]	✗	✓	✓**	✓**	✓	✗	✓	✗	✗
Groq	Gwennap [2020]	✗	✓	✗	✓	✓	✗	✗	✗	✗
Qualcomm AI100	Chatha [2021]	✗	✓	✗	✓	✓	✗	✗	✗	✗
Google TPU V4i	Jouppi et al. [2021]	✗	✓	✗	✓	✓	✗	✓	✗	✗
AMD MI300	AMD	✗	✓	✓	✓	✓	✓	✓	✓	✗
AMD AIE	Alok [2020]	✓	✓	✗	✓	✗	✗	✓	✗	✗

2 Background

Software and hardware Traditional software systems often employ measures to ensure that software executes exclusively on authorised hardware. This is achieved by integrating hardware identifiers, or fingerprints, into the software itself, and is similar to the methods presented in this paper. Upon execution, the software verifies the authenticity of the hardware it is running on by comparing its fingerprint to the expected value. Such fingerprints can be, for example, generated with Picasso by using web-browser agents and HTML canvases for identification [Bursztein et al., 2016], or DrawnApart, which relies on GPU speed variance [Laor et al., 2022].

Furthermore, comprehensive verification of the software and hardware loading process is frequently implemented. This involves employing secure boot-loaders, firmware checks, hardware authentication tokens, and platform modules to ensure the integrity of the system as a whole. By combining hardware fingerprinting with a thorough verification process, these systems can effectively restrict software execution to pre-approved hardware. Note, that all of the solutions are usually used in conjunction. In this paper we build examples of such mechanisms which are specifically suited for machine learning.

Machine Learning deployment Modern machine learning deployment primarily utilises centralised serving due to challenges in data sharing and the necessity for specialised hardware. In the realm of on-device inference, the prevailing approach to access and security management is through policy-based restrictions [Outchakoucht et al., 2017] and safety fine tuning [Qi et al., 2023].

2.1 Specialised Hardware

AI hardware vendors have designed a wide range of chips featuring a comprehensive range of hardware intrinsic supports. This often focuses on hardware arithmetic, optimisations such as sparsity, and security support like Trusted Execution Environment (TEE). Table 2 presents a compilation of recently developed AI accelerators along with their respective hardware intrinsic supports. It details features encompassing various arithmetic supports, including **INT4**, **INT8**, **FP8**, **FP16**, **FP32**, **TF32**, and **BFLOAT16**. Table 2 also considers the availability of support for sparse matrix multiplication (sparsity) and TEE in the devices listed. The device-level hardware intrinsic asymmetry, detailed in Table 2, provides substantial opportunities for its exploitation in hardware-locking. While software or compiler optimisations can imitate circuit design variations, these emulations *are inherently less efficient*, often by orders of magnitude, in terms of operation-per-Watt performance.

Furthermore, Table 2 illustrates how the same hardware support can vary in implementation. For instance, Tesla’s DOJO adopted distinctive **FP8** and **FP16** schemes, deviating from the conventional schemes, and termed them CFP. Notably, computations occur at finite precision, and the execution of the same operation often varies across hardware platforms. Consequently, even a standard **FP32** convolution operation might yield different numerical results on different hardware, as detailed by Schlögl et al. [2023]. The differences in hardware implementations and numerical deviations described above can also serve as sources of asymmetry for exploration in the realm of locking.

3 Methodology

3.1 Assumptions, Goals, and Definitions

The goal of this paper is to develop *locking* mechanisms that **make it hard to move a machine learning model from an authorised hardware platform to an unauthorised (different) hardware platform**. That is, to build mechanisms that deter unauthorised model use by restricting supported hardware. Note that our locks are not designed to replace existing cryptographic security solutions e.g. distribution and storage of encrypted weights, hardware security modules, and root of trust, but are rather developed to complement them for settings where restriction to specific hardware is preferred. Our methods are similar in function to standard encryption techniques, but use hardware-specific characteristics as key material, do not require explicit key management, and do not require dedicated cryptographic hardware.

In what follows, we explicitly separate two main types of locking: hard and soft. **Soft locking** mechanisms refer to mechanisms that do not fully restrict normal use of the model on non-authorised hardware, but rather make use of the model less performant or efficient. For example, consider a model that during inference produces abnormally large amounts of internal data that slows down inference on normal GPUs, but specialised GPUs filter the produced data to only keep task-informative data. **Hard locking** mechanisms refer to mechanisms that fully restrict use of models on non-authorised hardware, ideally with formal e.g. cryptographic guarantees. In practice, we envision both locking types to be used in conjunction. To make such mechanisms usable, we seek to minimise effort required to instrument the model for deployment. At the same time, given that both developing proprietary hardware platforms and training large-scale foundation models are expensive, we either opt to ① convert models into representations that are unique to specific platforms e.g. in Table 2 we show that **INT4** representation can be favourable for soft locking, since only two widely available hardware platforms support it; or ② condition models on hardware-specific behaviours e.g. introducing model dependency on latency of scatter/gather operations.

We explicitly note that **none of the mechanisms described in this paper on their own provide security** and could be circumvented by a knowledgeable attacker with enough effort and appropriate access. Furthermore, they in no way stop an adversary from performing model extraction, but these would result in significant adversary costs [Tramèr et al., 2016, Truong et al., 2021, Shafran et al., 2023]. Yet, our locks present a significant challenge for an attacker with locked model-only access.

3.2 Soft locking methods

Optimisations for model inference, such as pruning and quantisation, typically convert model parameters into sparse or low-precision tensors. These perturbations in the parameter space can lead to a test-time disparity, meaning that models, even if derived from the same original model but quantised with different arithmetics or pruned to varying sparsities, can misclassify distinct samples. Prior work has leveraged artefacts from quantisation or pruning to develop stealthy backdoor attacks [Ma et al., 2023, Hong et al., 2021]. Nonetheless, in *soft locking*, our interest lies in implementing strategies that enable optimisations *exclusively* on hardware platforms with specific intrinsic support, not on others. Unsupported or unauthorised hardware platforms may still be capable of running the same model but would suffer from inefficient execution and/or considerable performance degradation.

Sparsity-aware locking Pruning is a family of methods that transforms models with dense parameters into sparse ones [LeCun et al., 1989]. Pruning reduces the number of parameters needed to store the model and potentially decreases the amount of floating-point operations required, if supported by the hardware. Table 2 reveals that only NVIDIA A100, H100, Cerebras WSE2, and AMD MI300 possess hardware intrinsic support for sparse tensor acceleration, indicating the existence of hardware asymmetry in pruning. We propose a simple *fine-tuning* scheme to produce models that significantly degrade in performance when used at an unauthorised sparsity level. The loss for this proposed manipulation takes the form: $\mathcal{L} = \mathcal{L}(f_p(x, p_1), y) + \lambda(\epsilon - \mathcal{L}(f_p(x, p_2), y))^2$. Here $f_p(\cdot)$ represents the pruned version of the original network $f(\cdot)$, where x is the input and p_1 and p_2 are values between 0 and 1 that define the level of pruning in the pruned network. When $p = 0$, we have an unpruned, dense network. \mathcal{L} denotes a valid loss, for example cross-entropy. λ is a hyperparameter that allows tuning of the relative magnitudes of the original training term and the pruning-degradation term. ϵ denotes a target loss value for the pruned model. In essence, our loss promotes free optimisation for models with a sparsity p_1 while aiming to drive models with a sparsity p_2 toward a suboptimal

point, given that $p_1 \neq p_2$. This results in a sparsity-aware locking, where the model exhibits higher accuracy at a sparsity level of p_1 and significantly worse performance at a sparsity level of p_2 .

Quantisation-aware locking Machine Learning models are often distributed at lower quantisation to allow deployment on specialist or constrained hardware. ML locking could therefore be accomplished by limiting which quantisations a particular model could be run at. We propose using a loss similar to the pruning-degradation loss defined above and that used by Hong et al. [2021] to backdoor models, in order to lock the quantisation levels which a model can be used on. The differences between our aim and Hong et al. [2021] are two-fold. Firstly, we aim to make transferring across hardware systems more challenging in order to accomplish ML locking instead of trying to backdoor model quantisation. Secondly, we expand upon the approach of Hong et al. [2021] across various arithmetic types, not just within the integer arithmetic domain, as many chips listed in Table 2 support integer arithmetic but vary in their support for different floating-point or even custom arithmetics.

3.3 Hard locking methods

Our *hard locking* methods are based on using a fingerprint obtained from a specific device to transform model parameters in a way that is difficult to invert without the fingerprint. Note that such signatures can be shared across devices from the same family, as we show with clock fingerprints, as well as, specific individual devices as we show with finite precision fingerprints.

First, the properties of the target device model are used to generate a *high-entropy fingerprint* unique to the device or the device model, which is hard or impossible to replicate from other devices or device families. Then, a *parameter transformation function* is used to modify the model parameters based on the fingerprint. The model is only ever stored in its transformed form, and detransformed on the fly by the authorised device. Without knowledge of the fingerprint, the transformed model is not functional, and the fingerprinting method is designed to have high entropy, such that it cannot easily be guessed or brute-forced without access to the authorised hardware.

Device fingerprinting The fingerprinting method can be anything which produces a consistent and unguessable output on one device or device model but a different output on other devices. It should have sufficient entropy to produce sufficient key material for the encryption-like parameter transformations. We propose three candidate device fingerprints: the *clock fingerprint*, the *finite precision fingerprint*, and the *PUF fingerprint*. Different methods can be combined together for additional entropy.

Clock fingerprint The *clock fingerprint* is generated by counting the number of clock cycles taken by a CUDA device to repeatedly add numbers together. The fingerprint is this number represented as five symbols of hexadecimal. This can be seen in Table 3. We find experimentally that the GP102 produces an output stochastically between 72100 and 723ff, while the TU102 and GA102 produce a fingerprint deterministically. The entropy of the clock fingerprint is upper bounded by the number of bits in the output (20). Clock fingerprints are an example of device-family fingerprint. We show our clock fingerprint generator in Appendix J.

Table 3: Clock fingerprint on various devices

Device	GPU	Fingerprint
GTX 1080Ti	GP102	72100 to 723ff
RTX 2080Ti	TU102	49a59
RTX 3090	GA102	4b85a
RTX A6000	GA102	4b85a

Finite precision fingerprint The *finite precision fingerprint* is generated via numerical errors specific to an arithmetic and precision. In ML systems, these can also occur due to inference-time microbenchmarking [Schlögl et al., 2023]. Device-specific ML framework implementation choices produce a unique error which can be used as a fingerprint. The total entropy is determined by the total number of possible sets of such choices. Schlögl et al. [2023] find a maximum of four error equivalence classes, or two bits of entropy, for a single convolution. The total bits of entropy available in a convolution-based finite precision fingerprint is therefore upper bounded by twice the number of convolutions performed. In reality, a large number of bits would be difficult to obtain due to strong correlations between the algorithm choices. At the same time, we find that floating point operations in general can be used to generate device-specific errors. We compute a finite precision fingerprint based on the SHA-256 hash of the error generated in a sequence of linear layers. These can be seen in Appendix I. We find that the fingerprint is consistent between different GPUs of the same model

on the same system, but differ between systems. This could be used to further lock models to other components of the system. We show our precision fingerprint generator in Appendix K.

PUF fingerprint Physically Unclonable Functions (PUFs) that exist in (or are explicitly introduced into) hardware can be used to derive a high-entropy device fingerprint. For example, Van Aubel et al. [2015] finds that the initial state of shared SRAM memory in NVIDIA GPUs is one example of an un-advertised PUF, while other constructions are possible [Li et al., 2015, Forlin et al., 2020]. These PUFs could be combined with fuzzy extractors [Dodis et al., 2004] to achieve a reliable fingerprint. In model-distributed setups, these PUFs could be chained together across multiple devices.

Parameter transformation In order to achieve *hard locking*, we must transform the model parameters in a way that can only be easily inverted with knowledge of the fingerprint. There are three ideal properties of the transformation, defined informally as follows:

1. **Destruction:** The performance of a model with transformed parameters or parameters detransformed with an incorrect fingerprint should be significantly hampered, ideally equivalent to random guessing. Without destruction, the model would still be usable without the fingerprint, and hard locking fails.
2. **Encryption:** No information about the original parameters should be obtainable from the transformed parameters, other than the information required for *indistinguishability*. If encryption holds, then the attacker must brute-force all possible fingerprints to determine the correct one to reveal the secret. If it does not, in some cases cheaper methods such as gradient descent may be applicable for extracting the original parameters.
3. **Indistinguishability:** Incorrectly detransformed parameters should be statistically indistinguishable in aggregate from correct parameters. If indistinguishability holds, then in a brute-force attack the attacker must run each candidate model on test data and choose the correct one by maximising test accuracy. This is in general more expensive and error-prone than a statistical test.

Table 4 considers three parameter transformation methods in terms of these properties: *AES encryption*, *Parameter shuffling*, and *Pre-transformed AES encryption*. These are described below.

AES Encryption The obvious method to transform the model parameters is with a classical encryption scheme, this gives rise to the *AES encryption* method, in which the parameters of the model are collected together into a bytestream, which is then AES-encrypted, keyed by the SHA-256 hash of the fingerprint. The resulting bytestream is then the transformed parameters. This achieves perfect *encryption* and *destruction*, but not *indistinguishability*, because incorrectly decrypted parameters will be uniformly distributed, in contrast to the correct parameters.

In conventional cryptographic schemes, security can be increased by using higher-entropy keys to make brute-forcing infeasible. Since the entropy of a fingerprint is fixed and cannot be increased, we focus instead on making each decryption attempt more expensive, i.e. key-stretching [Kelsey et al., 1997]. We propose achieving this through *indistinguishability*. With indistinguishability, for each candidate fingerprint the attacker must evaluate the candidate model’s accuracy, which is computationally expensive. Indistinguishability of parameters is feasible since the statistics of ML parameters are much easier to fake than the plaintext of most encryption schemes (for example, coherent English text, or a valid JPEG file).

In order to achieve *indistinguishability* and thus make a brute-force attack more difficult, we developed two further transformation methods: *parameter shuffling*, and *pre-transformed AES encryption*.

Parameter shuffling In the *parameter shuffling* method, the fingerprint is used as a seed to generate a random permutation of the parameters, which is then used in place of the original parameters. This achieves near-perfect *indistinguishability* and *destruction*, but does not achieve *encryption*, as some information about the original parameters still exists in the permuted parameters.

Table 4: Comparison of parameter transformations that can be applied with different fingerprints.

Method	Indistinguishability	Encryption	Destruction
AES encryption	✗	✓	✓
Parameter shuffling	✓	✗	✓
Pre-transformed AES encryption	✓	✓	✓

In practice, however, because the search space of permutations (factorial of the number of parameters) is many orders of magnitude larger than the search space of keys (two to the power of the fingerprint entropy), it is much more efficient for an attacker to brute force the key space than attempt gradient descent in the permutation space, and so the lack of perfect encryption is unimportant. For example, a very large fingerprint with 256 bits of key material has a search space of $2^{256} \approx 10^{80}$, but even a small ResNet18 test model has over 10^7 parameters, equating to a permutation search space of $(10^7)! \approx 10^{10^8}$, untenably larger.

Pre-transformed AES encryption The problem with naïve AES transformation is that incorrectly detransformed parameters are uniformly distributed in byte-space, while correct parameters have some other distribution, often Gaussian, making cracking considerably easier.

We can correct for this problem by defining an additional transformation function, the ‘pre-transformation’ function. This is applied to the parameters before encryption, such that these parameters are then uniform in byte-space, and indistinguishable from incorrectly decrypted bytes. This pre-transformation function is reversed after decryption.

The sole purpose of the pre-transformation function is to achieve *indistinguishability* by transforming the uniform distribution of incorrectly decrypted AES to the same distribution as the correct parameters. It must be stored unencrypted to prevent distinguishability by statistics on the pre-transformation. We therefore say that the pre-transformed AES encryption transformation achieves the full trifecta of *indistinguishability*, *encryption*, and *destruction*.

A generic distribution can be pre-transformed to be uniform by applying its cumulative distribution function to it. For example, if X , the distribution of model parameters, is Gaussian with mean μ and variance σ^2 , then Y , the distribution of pre-transformed model parameters, is uniform in the region $(0, 1)$, where $Y = \frac{1}{2} \left[1 + \operatorname{erf} \left(\frac{X-\mu}{\sigma\sqrt{2}} \right) \right]$. If Y is then encoded as integers spanning the full possible integer range, its distribution will also be uniform in byte space, and thus indistinguishable from incorrectly decrypted bytes.

We evaluated pre-transforming the parameters of a test ResNet18 model trained on CIFAR10, first by assuming that it was Gaussian, and secondly by directly estimating the cumulative distribution function via sampling of the parameters. This can be seen in Appendix H.

In practice, assuming that the distribution is Gaussian may be problematic. If there are any outliers, then applying the cumulative distribution function will take these outliers so close to 0 or 1 that they can no longer be represented with sufficient precision in floating point, and they will become exactly 0 or 1. Then, these outliers detransform to positive or negative infinity, destroying the model. There are sufficiently many outliers that subsequently casting these outliers to any fixed finite value will destroy the accuracy of the model. Regardless of any scheme to correct for this, *indistinguishability* is broken, because these infinities do not occur with comparable frequency in incorrectly detransformed data.

To fix this problem, we instead computed the cumulative distribution function of the parameters empirically, then used this as a look-up table to transform the distribution into a uniform distribution. For an n -bit precision, computing the pre-transformation requires $\mathcal{O}(2^n)$ time and space, but applying the pre-transformation or de-pre-transformation is cheap. This is computationally tractable for precisions up to 32-bits and inexpensive for precisions up to 16-bit. The results for FP16 can be seen in Figure 16 in Appendix H. There exists a trade-off between the pre-transform being exactly invertible and it exactly matching the target distribution for random data. Reported results are for an exact pre-transformation.

4 Evaluation

4.1 Evaluating soft locking

We evaluate the effects of different soft locking schemes as illustrated in Table 1. When run on unauthorised hardware, soft-locked models will cause either a slow down in inference, or a drop in accuracy or model performance. The former occurs because unauthorised hardware may emulate the execution of authorised hardware at the software level, due to a lack of hardware intrinsic support, this will result in slowdowns, as we evaluate in Section 4.1.3. Alternatively, if unauthorised hardware

directly executes only what is natively supported, it would incur an accuracy penalty, as illustrated in Section 4.1.1, and Section 4.1.2.

4.1.1 Performance degradation for sparsity-aware lock

We investigate sparsity-aware locking, for the widely-used l_1 -unstructured pruning [LeCun et al., 1989, Li et al., 2017] across pruning levels (0.05, 0.10, 0.25, 0.50, 0.75) for both vision and language models, across different datasets. For all vision models, we fine-tune a trained model ² with the loss defined in Section 3.2 for 25 epochs, with $\lambda = 1$ and $\epsilon = 5$. The language models are fine-tuned for 3 epochs, as this was sufficient for effective manipulation.

We fine-tuned the BERT model [Devlin et al., 2019], and specifically the *bert-base-cased-finetuned- $\{sst2, cola, mrpc\}$* HuggingFace checkpoints on the respective GLUE tasks [Wang et al., 2018], with the pruning-resistant loss from Section 3.2. We also evaluate performance on various vision tasks such as CIFAR10, CIFAR100 [Krizhevsky and Hinton, 2009], and Flowers102 [Nilsback and Zisserman, 2008], utilising ResNet18, ResNet50 [He et al., 2016], and ViT-B [Dosovitskiy et al., 2021] for these specific tasks.

Table 5 displays sparsity-aware lock results, we present the following metrics as illustrated in Figure 2:

- $Acc_{\text{authorised}}^{\text{locked}}$: the accuracy of models with soft locks running on authorised hardware.
- $\Delta_{\text{orig}} = Acc_{\text{original}} - Acc_{\text{authorised}}^{\text{locked}}$ measures the impact of soft locking on authorised execution by comparing the accuracy of the original model (without locks) to that of the locked model executing on authorised hardware. A **small** Δ_{orig} value is desirable.
- $\Delta_{\text{lock}} = Acc_{\text{authorised}}^{\text{locked}} - Acc_{\text{unauthorised}}^{\text{locked}}$ measures the degradation in accuracy when locked models are deployed on unauthorised devices. A **large** Δ_{lock} value is desirable.

Table 5 demonstrates that sparsity-aware lock leaves the accuracy of the authorised execution largely unaffected, as shown by the small Δ_{orig} values. Meanwhile, locked models experience significant accuracy degradation when operating on unauthorised hardware, as indicated by the substantial Δ_{lock} values. We present the accuracy drop from hardware transfer without locking, Δ_{base} , in the Appendix (F). It is clear that the significant accuracy drop from transfer can be attributed to locking (and not merely pruning), as the degradation in accuracy of the original models, Δ_{base} , is generally much lower than that of the locked models, Δ_{lock} . Certain settings, such as *BERT* on MRPC, show that the sparsity-aware lock can trigger a larger degradation in performance when the unauthorised configuration is more sparse (i.e. greater pruning proportion, p). However, even a low unauthorised pruning proportion of $p = 0.05$ is sufficient for sparsity-aware locks to be effective.

An obvious attack on the sparsity-lock is re-training with a pruning-aware loss on the unauthorised hardware. We investigate the recovery accuracy in G.2, and find that at lower levels of sparsity, p (0.05 and 0.25), re-training does not allow the model to reach the accuracy of the original (i.e. unlocked) model running on unauthorised hardware. At $p = 0.50$, accuracy is regained after roughly 5 epochs. As such, the locking procedure is highly effective, as in the best case it causes terminal damage, and otherwise, it necessitates further training from the unauthorised users, who may not have access to the training data. We present further investigation in the Appendix (G, F.3), including into the specificity of locking to the assumed unauthorised sparsity level, and typical locking profiles.

²Training and fine-tuning hyper-parameters presented in the Appendix D.

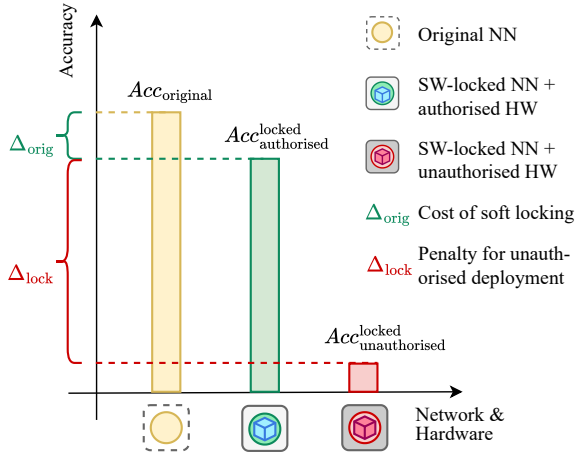


Figure 2: Applying soft locks to a model with Acc_{original} , Δ_{orig} and Δ_{lock} measure together the effectiveness of locking.

Table 5: Results are presented as $Acc_{\text{authorised}}^{\text{locked}}(\Delta_{\text{orig}}, \Delta_{\text{lock}})$.

Dataset	Pruning Levels		
	0.05	0.25	0.50
<i>BERT</i>			
CoLA	0.80 (-0.03, 0.49)	0.84 (0.00, 0.53)	0.83 (0.00, 0.53)
MRPC	0.84 (-0.02, 0.15)	0.86 (0.00, 0.18)	0.86 (0.00, 0.54)
SST-2	0.92 (-0.01, 0.43)	0.93 (0.00, 0.43)	0.92 (0.00, 0.43)
<i>Resnet18</i>			
CIFAR10	0.89 (0.03, 0.67)	0.93 (0.00, 0.83)	0.93 (0.00, 0.83)
CIFAR100	0.73 (0.03, 0.71)	0.76 (0.00, 0.75)	0.76 (0.00, 0.75)
Flowers102	0.84 (0.04, 0.83)	0.89 (0.00, 0.88)	0.89 (0.00, 0.88)
<i>Resnet50</i>			
CIFAR10	0.92 (0.01, 0.81)	0.93 (-0.01, 0.83)	0.94 (-0.01, 0.84)
CIFAR100	0.69 (0.09, 0.63)	0.78 (0.00, 0.77)	0.78 (0.00, 0.77)
Flowers102	0.76 (0.10, 0.74)	0.86 (0.00, 0.84)	0.86 (0.00, 0.84)
<i>ViT-B_16-224</i>			
CIFAR10	0.99 (0.00, 0.89)	0.99 (0.00, 0.89)	0.99 (0.07, 0.89)
CIFAR100	0.92 (-0.02, 0.92)	0.93 (-0.02, 0.92)	0.93 (-0.02, 0.93)
Flowers102	1.00 (0.00, 0.98)	1.00 (0.00, 0.99)	1.00 (0.00, 0.99)

Table 6: Results are presented as $Acc_{\text{authorised}}^{\text{locked}}(\Delta_{\text{orig}}, \Delta_{\text{lock}})$.

authorised \rightarrow Unauthorised	Resnet18	Resnet50
FP32 \rightarrow 8-bit MiniFloat	0.90 (-0.02, 0.65)	0.92 (-0.04, 0.67)
Int8 \rightarrow 8-bit MiniFloat	0.47 (+0.41, 0.06)	0.50 (+0.39, 0.07)
FP16 \rightarrow Int8	0.90 (-0.02, 0.62)	0.91 (-0.04, 0.61)
16-bit MiniFloat ³ \rightarrow Int8	0.90 (-0.01, 0.72)	0.91 (-0.03, 0.81)

4.1.2 Performance degradation for quantisation-aware lock

We investigate quantisation-aware locking on ResNet models across a set of authorised, unauthorised arithmetic pairs, using the quantisation-aware locks described in Section 3.2. The models are trained for 25 epochs, with $\lambda = 1$ and $\epsilon = 5$, as with sparsity-aware locking. We note that Hong et al. [2021] previously used a similar loss in Section 3.2 to learn models that degrade upon quantisation to a lower precision. We extend this by investigating the effectiveness of preventing transfer across both precision and arithmetics and present the results below, using the metrics from Section 4.1.1.

Here, we use FP32 to simulate these formats during fine-tuning to prove the idea, which is independent of hardware. In both models, the quantization-aware lock causes performance to degrade to near-random guessing performance when the quantization is *to a lower precisions than the original model*, as evident by both **FP32 to 8-bit MiniFloat** and **16-bit MiniFloat³ to Int8** in Table 6. Manipulation across the same precision, but different arithmetic, was not successful (**Int8 to 8-bit MiniFloat**), showing there is not sufficient discrepancy in their representations for this simple manipulation procedure to yield model degradation. However, the transfer across arithmetics (**16-Bit MiniFloat to Int8**) results in a greater degradation, with a lower difference in precision than transfer across just precision (**FP32 to 8-bit MiniFloat**).

4.1.3 Emulation cost for soft locking

As described in Section 3.2 and shown in Table 1, unauthorised devices without supported hardware intrinsics may opt for operation emulation, which incurs additional throughput costs. For a fair comparison, we assess the performance of both a single matrix multiplication operation (`matmul`) and the prefill phase of the entire network with and without software emulation on the same device, an NVIDIA A6000 GPU. In Table 7, for sparsity-aware locking, the term “**Real**” signifies that weight matrices exhibit a sparsity level of 0.995, implemented via `torch.sparse.mm`. Conversely, “**Emulated**” indicates that the linear layer employs a full weight matrix alongside a 0.995-sparsity mask; during runtime, this mask is applied to the weights, which are then processed using `nn.functional.linear`. Regarding quantisation-aware lock, “**Real**” means the hardware

³Besides FP16, vendors have various MiniFloat formats, such as Google’s **BFloat16** and NVidia’s **TensorFloat**. Here we set an exponent width of 5 and an exponent bias of 11.

Table 7: Emulation costs for soft locking. Though the accuracy of soft locked model can be recovered by emulation on unauthorised hardware, the inference suffers from inefficient execution, such as a lower throughput and higher latency. The single matmul is at a size of (2048, 2048), and we use the OPT-2.7B model at a batch size of 4 on NVIDIA A6000. TOPS denotes Tera operations per second, and TPS is tokens per second.

Workload	Metric	Sparsity-aware		Quantization-aware	
		Real	Emulated	Real	Emulated
Single Matmul	Throughput (TOPS)	49.97	18.85	79.22	22.72
	Latency (ms)	0.43	1.14	0.27	0.95
OPT inference	Throughput (TPS)	4692.20	2468.31	3505.22	1865.41
	Latency (ms)	436.47	829.72	584.27	1097.88

executes the quantised operation using its intrinsically supported INT8 GEMM, where “**Emulated**” is emulating the INT8 operations using ordinary FP32 operations. We use the MASE flow for both sparsity and quantisation emulations [Cheng et al., 2023]. We consider both a single matrix multiply as the size of (2048, 2048) and a full OPT-2.7B model inference at a batch size of 4.

Our results in Section 3.2 suggest that emulation comes at a large cost. For instance for a single matrix multiply, both sparsity-aware and quantisation-aware locks induce a $2.65\times$ and $3.52\times$ overhead in latency, and a $2.65\times$ and $3.49\times$ reduction in throughput. For the inference of OPT-2.7B, the emulation overhead is around $2\times$ in both latency and throughput.

4.2 Hard locking

We tested the three transformation functions presented in Section 3.3 on ResNet18 [He et al., 2016] trained on CIFAR10 [Krizhevsky and Hinton, 2009]. All three successfully achieve *destruction*, as can be seen in Table 8. We further tested the cost to fully brute force each. In our tests on this very small model, the *indistinguishability* property of the *Parameter shuffling* and *Pre-transformed AES* methods added to the cracking cost by just under one order of magnitude. In a larger and more expensive to evaluate model, we expect the difference to be several orders of magnitude.

Table 8: Accuracy of test model (FP16 ResNet18 trained on CIFAR10) with parameter transformations. 10% is random guessing. “Correctly detransformed” is detransformed with the same fingerprint that was transformed with, while “Incorrectly detransformed” is detransformed with any other fingerprint. Cost refers to experimental cost of model extraction on a toy model (CPU hours for full brute-force). b is the number of bits of entropy in the fingerprint, discussed further in Appendix B.

Method	Accuracy				Cracking cost (s)
	Original	Transformed	Correctly detransformed	Incorrectly detransformed	
AES encryption	95.4%	10%	95.4%	10%	0.3×2^b
Parameter shuffling	95.4%	10%	95.4%	10%	2.7×2^b
Pre-transformed AES encryption	95.4%	10%	95.4%	10%	1.3×2^b

5 Conclusion

In this paper we introduce *machine learning locking*, a novel paradigm for safeguarding machine learning models from unauthorised use to address a growing concern about intellectual property protection and responsible AI use. We investigate a number of different locking mechanisms, encompassing both soft locking, which discourages model theft by imposing performance penalties on unauthorised hardware, and hard locking, which leverages hardware fingerprints to (cryptographically) bind models to specific platforms. Our experiments demonstrated the effectiveness of these locking mechanisms, both in preserving model performance and introducing significant complexity in removing the locks. By investigating hardware-based locking mechanisms, we offer a potential solution for safeguarding valuable on-device ML models.

References

- AMD Instinct MI300 Series Accelerators. <https://www.amd.com/en/products/accelerators/instinct/mi300.html>. Accessed: 2024-03-03.
- G. Alok. Architecture apocalypse dream architecture for deep learning inference and compute-versal ai core. *Embedded World*, 2020.
- T. Brown, B. Mann, N. Ryder, M. Subbiah, J. D. Kaplan, P. Dhariwal, A. Neelakantan, P. Shyam, G. Sastry, A. Askell, S. Agarwal, A. Herbert-Voss, G. Krueger, T. Henighan, R. Child, A. Ramesh, D. Ziegler, J. Wu, C. Winter, C. Hesse, M. Chen, E. Sigler, M. Litwin, S. Gray, B. Chess, J. Clark, C. Berner, S. McCandlish, A. Radford, I. Sutskever, and D. Amodei. Language Models are Few-Shot Learners. In *Advances in Neural Information Processing Systems (NIPS)*, pages 1877–1901. Curran Associates, Inc., 2020. URL https://proceedings.neurips.cc/paper_files/paper/2020/file/1457c0d6bfc4967418bfb8ac142f64a-Paper.pdf.
- E. Bursztein, A. Malyshev, T. Pietraszek, and K. Thomas. Picasso: Lightweight device class fingerprinting for web clients. In *Proceedings of the 6th Workshop on Security and Privacy in Smartphones and Mobile Devices (SPSM)*, pages 93–102, 2016.
- K. Chatha. Qualcomm® Cloud AI 100: 12TOPS/W Scalable, High Performance and Low Latency Deep Learning Inference Accelerator. In *2021 IEEE Hot Chips 33 Symposium (HCS)*, pages 1–19. IEEE, 2021.
- J. Cheng, C. Zhang, Z. Yu, A. Montgomerie-Corcoran, C. Xiao, C.-S. Bouganis, and Y. Zhao. Fast Prototyping Next-Generation Accelerators for New ML Models using MASE: ML Accelerator System Exploration. *arXiv preprint arXiv:2307.15517*, 2023.
- J. Choquette. NVIDIA Hopper H100 GPU: Scaling Performance. *IEEE Micro*, (3):9–17, 2023.
- J. Choquette, W. Gandhi, O. Giroux, N. Stam, and R. Krashinsky. NVIDIA A100 tensor core GPU: Performance and innovation. *IEEE Micro*, (2):29–35, 2021.
- J. Devlin, M. Chang, K. Lee, and K. Toutanova. BERT: Pre-training of Deep Bidirectional Transformers for Language Understanding. In *Proceedings of the 2019 Conference of the North American Chapter of the Association for Computational Linguistics: Human Language Technologies (NAACL-HLT)*, pages 4171–4186. Association for Computational Linguistics, 2019. URL <https://doi.org/10.18653/v1/n19-1423>.
- Y. Dodis, L. Reyzin, and A. Smith. Fuzzy Extractors: How to Generate Strong Keys from Biometrics and Other Noisy Data. In *Advances in Cryptology - EUROCRYPT 2004*, pages 523–540. Springer Berlin Heidelberg, 2004.
- A. Dosovitskiy, L. Beyer, A. Kolesnikov, D. Weissenborn, X. Zhai, T. Unterthiner, M. Dehghani, M. Minderer, G. Heigold, S. Gelly, J. Uszkoreit, and N. Houlsby. An Image is Worth 16x16 Words: Transformers for Image Recognition at Scale. In *9th International Conference on Learning Representations (ICLR)*. OpenReview.net, 2021. URL <https://openreview.net/forum?id=YicbFdNTTy>.
- C. M. Ferrandis. Openrail: Towards open and responsible AI licensing frameworks, 2022. URL <https://www.licenses.ai/faq-2>.
- B. Forlin, R. Husemann, L. Carro, C. Reinbrecht, S. Hamdioui, and M. Taouil. G-PUF: An Intrinsic PUF Based on GPU Error Signatures. In *2020 IEEE European Test Symposium (ETS)*, pages 1–2, 2020.
- L. Gwennap. Groq rocks neural networks. *Microprocessor Report, Tech. Rep.*, jan, 2020.
- G. K. Hadfield and J. Clark. Regulatory Markets: The Future of AI Governance. *arXiv preprint arXiv:2304.04914*, 2023.
- K. He, X. Zhang, S. Ren, and J. Sun. Deep Residual Learning for Image Recognition. In *Proceedings of the IEEE conference on computer vision and pattern recognition (CVPR)*, pages 770–778, 2016.

- P. Henderson, E. Mitchell, C. Manning, D. Jurafsky, and C. Finn. Self-Destructing Models: Increasing the Costs of Harmful Dual Uses of Foundation Models. In *Proceedings of the 2023 AAAI/ACM Conference on AI, Ethics, and Society*, AIES '23, page 287–296. Association for Computing Machinery, 2023. URL <https://doi.org/10.1145/3600211.3604690>.
- S. Hong, M.-A. Panaitescu-Liess, Y. Kaya, and T. Dumitras. Qu-ANTI-zation: Exploiting Quantization Artifacts for Achieving Adversarial Outcomes. In *Advances in Neural Information Processing Systems (NIPS)*, pages 9303–9316. Curran Associates, Inc., 2021. URL https://proceedings.neurips.cc/paper_files/paper/2021/file/4d8bd3f7351f4fee76ba17594f070ddd-Paper.pdf.
- N. P. Jouppi, D. H. Yoon, M. Ashcraft, M. Gottscho, T. B. Jablin, G. Kurian, J. Laudon, S. Li, P. Ma, X. Ma, et al. Ten Lessons from Three Generations Shaped Google’s TPUv4i: Industrial Product. In *2021 ACM/IEEE 48th Annual International Symposium on Computer Architecture (ISCA)*, pages 1–14. IEEE, 2021.
- J. Kelsey, B. Schneier, C. Hall, and D. Wagner. Secure applications of low-entropy keys. In *International Workshop on Information Security*, pages 121–134. Springer, 1997.
- A. Krizhevsky and G. Hinton. Learning Multiple Layers of Features from Tiny Images. Technical report, University of Toronto, 2009. URL <https://www.cs.toronto.edu/~kriz/learning-features-2009-TR.pdf>.
- T. Laor, N. Mehanna, A. Durey, V. Dyadyuk, P. Laperdrix, C. Maurice, Y. Oren, R. Rouvoy, W. Rudametkin, and Y. Yarom. DRAWN APART: A Device Identification Technique based on Remote GPU Fingerprinting. In *Proceedings 2022 Network and Distributed System Security Symposium (NDSS)*, NDSS 2022. Internet Society, 2022. URL <http://dx.doi.org/10.14722/ndss.2022.24093>.
- Y. LeCun, J. Denker, and S. Solla. Optimal Brain Damage. In *Advances in Neural Information Processing Systems (NIPS)*. Morgan-Kaufmann, 1989. URL https://proceedings.neurips.cc/paper_files/paper/1989/file/6c9882bbac1c7093bd25041881277658-Paper.pdf.
- F. Li, X. Fu, and B. Luo. POSTER: A Hardware Fingerprint Using GPU core frequency variations. In *Proceedings of the 22nd ACM SIGSAC Conference on Computer and Communications Security, CCS '15*, page 1650–1652. Association for Computing Machinery, 2015. URL <https://doi.org/10.1145/2810103.2810105>.
- H. Li, A. Kadav, I. Durdanovic, H. Samet, and H. P. Graf. Pruning Filters for Efficient ConvNets. In *5th International Conference on Learning Representations (ICLR)*. OpenReview.net, 2017. URL <https://openreview.net/forum?id=rJqFGTslg>.
- Z. Lin, J. Cui, X. Liao, and X. Wang. Malla: Demystifying Real-world Large Language Model Integrated Malicious Services. *arXiv preprint arXiv:2401.03315*, 2024.
- H. Ma, H. Qiu, Y. Gao, Z. Zhang, A. Abuadba, M. Xue, A. Fu, J. Zhang, S. F. Al-Sarawi, and D. Abbott. Quantization Backdoors to Deep Learning Commercial Frameworks. *IEEE Transactions on Dependable and Secure Computing*, 2023.
- M.-E. Nilsback and A. Zisserman. Automated flower classification over a large number of classes. In *2008 Sixth Indian conference on computer vision, graphics & image processing*, pages 722–729. IEEE, 2008.
- NVIDIA. NVIDIA Nvidia Data Center GPU Resource Center. <https://resources.nvidia.com/1/en-us-gpu>. Accessed: 2024-22-05.
- A. Outchakoucht, E.-S. Hamza, and J. P. Leroy. Dynamic access control policy based on blockchain and machine learning for the internet of things. *International journal of advanced Computer Science and applications*, 8(7), 2017.
- X. Qi, Y. Zeng, T. Xie, P.-Y. Chen, R. Jia, P. Mittal, and P. Henderson. Fine-tuning aligned language models compromises safety, even when users do not intend to! *arXiv preprint arXiv:2310.03693*, 2023.

- A. Schlögl, N. Hofer, and R. Böhme. Causes and Effects of Unanticipated Numerical Deviations in Neural Network Inference Frameworks. In *Advances in Neural Information Processing Systems (NIPS)*, pages 56095–56107. Curran Associates, Inc., 2023. URL https://proceedings.neurips.cc/paper_files/paper/2023/file/af076c3bdbf935b81d808e37c5ede463-Paper-Conference.pdf.
- J. Selig. The cerebrus software development kit: A technical overview. 2022.
- A. Shafraan, I. Shumailov, M. A. Erdogdu, and N. Papernot. Beyond Labeling Oracles: What does it mean to steal ML models?, 2023.
- E. Talpes, D. Williams, and D. D. Sarma. DOJO: The Microarchitecture of Tesla’s Exa-Scale Computer. In *2022 IEEE Hot Chips 34 Symposium (HCS)*, pages 1–28, 2022.
- H. Touvron, L. Martin, K. Stone, P. Albert, A. Almahairi, Y. Babaei, N. Bashlykov, S. Batra, P. Bhargava, S. Bhosale, et al. Llama 2: Open foundation and fine-tuned chat models. *arXiv preprint arXiv:2307.09288*, 2023.
- F. Tramèr, F. Zhang, A. Juels, M. K. Reiter, and T. Ristenpart. Stealing Machine Learning Models via Prediction APIs. In *25th USENIX Security Symposium (USENIX Security 16)*, pages 601–618. USENIX Association, 2016. URL <https://www.usenix.org/conference/usenixsecurity16/technical-sessions/presentation/tramer>.
- J.-B. Truong, P. Maini, R. J. Walls, and N. Papernot. Data-Free Model Extraction. In *Proceedings of the IEEE/CVF conference on computer vision and pattern recognition (CVPR)*, pages 4771–4780, 2021.
- P. Van Aubel, D. J. Bernstein, and R. Niederhagen. Investigating SRAM PUFs in large CPUs and GPUs. In *Security, Privacy, and Applied Cryptography Engineering*, pages 228–247. Springer International Publishing, 2015.
- J. Vincent. Meta’s powerful AI language model has leaked online — what happens now?, 2023. URL <https://www.theverge.com/2023/3/8/23629362/meta-ai-language-model-llama-leak-online-misuse>.
- A. Wang, A. Singh, J. Michael, F. Hill, O. Levy, and S. Bowman. GLUE: A Multi-Task Benchmark and Analysis Platform for Natural Language Understanding. In *Proceedings of the 2018 EMNLP Workshop BlackboxNLP: Analyzing and Interpreting Neural Networks for NLP*, pages 353–355. Association for Computational Linguistics, 2018. URL <https://aclanthology.org/W18-5446>.

6 Appendix / supplemental material

A Broader Impact

Our research addresses the growing need to protect machine learning models from misuse. By introducing the concept of machine learning locking, our work offers a new tool to safeguard machine learning IP and aids responsible ML development and deployment. Our work also has implications for the governance of ML. By connecting models to specific hardware, another tool becomes available to control where and how such models are used. This could be particularly valuable in safety-critical applications, where ensuring that models are only executed in authenticated settings is paramount.

B Hard Locking and Entropy estimates

Results are presented in Table 9. Here, we list 20 as a strict upper bound for the clock fingerprint as it is the number of bits in the output. We expect the real entropy to still be considerable to provide useful security guarantees, but cannot estimate it without a large-scale experiment on diverse hardware.

Twice the number of convolutions is a theoretical result based on Schlögl et al. [2023]’s work which finds four equivalence classes for each convolution performed. It is an upper bound for a convolution-based finite precision fingerprint, but convolution is not the only possible strategy for a finite precision

fingerprint, indeed our finite precision fingerprints in Appendix K and Appendix I are not based on convolutions. The entropy of the SRAM PUF is an experimental result [Van Aubel et al., 2015], theoretically more than 256 is possible, but in our implementation encryption schemes we assume 256 bits, so any further entropy is not applicable.

Table 9: Comparison of methods of generating fingerprints from hardware. * estimated

Method	Entropy (bits)	Error rate
Clock	20 (upper bound)	<0.1%
Finite precision	$2 \times \text{num. of convolutions}$ (theoretical)	5%*
SRAM PUF [Van Aubel et al., 2015]	>256	5%*

C Base-model Training

Sparsity-aware lock We use open-source SoTA setups for training the base models in soft locking experiments:

- We use an open-source Github checkpoint⁴ as the base model for *ResNet18/50* on CIFAR10. For *ResNet18/50* on CIFAR100 and Flowers102, we train the models from scratch using the open-source scripts⁵. We adopt their hyperparameter settings except that we resize the Flowers102 images to 128×128 .
- We download *ViT-B_16-224* checkpoint from an open-sourced Github repository⁶ and fine-tune it using the scripts and hyperparameters provided in the same repository. All images are resized to 224×224 during training.
- We download *bert-base-cased* checkpoint from HuggingFace⁷, and use the default hyperparameters provided in the sequence classification training script open-sourced in the transformers repository⁸.

Quantisation-aware lock We use the same checkpoints and settings for quantisation-aware locking experiments. The checkpoints were trained for 50 epochs with a quantisation-aware loss using AdamW with a learning-rate of $1e^{-3}$, a batch size of 256, and a random seed of 0.

D Soft-locking Fine-Tuning

We use AdamW with a learning-rate of $1e^{-5}$ for both soft-locking procedures. *ViT-B_16-224* and the *ResNet* models were locked with batch-sizes of 32 and 256 respectively. Flowers102 images were resized to 128×128 for the ResNet models, and all datasets were resized to 224×224 for *ViT-B_16-224*. All runs were seed with random seed 0.

E Sparsity-Aware Lock - Extended Table 5

We present below a finer version of 5 below, with two extra sparsity levels, $p = 0.10, 0.25$, for completeness.

⁴Github repository: huyvnphan/PyTorch_CIFAR10

⁵Github repository: weiaicunzai/pytorch-cifar100

⁶Github repository: jeonsworld/ViT-pytorch

⁷HuggingFace checkpoint: google-bert/bert-base-cased

⁸HuggingFace transformer: run_glue.py for sequence classification

Table 10: Results are presented as $Acc_{\text{authorised}}^{\text{locked}}(\Delta_{\text{orig}}, \Delta_{\text{lock}})$

Dataset	Pruning Levels				
	0.05	0.10	0.25	0.50	0.75
<i>BERT</i>					
CoLA	0.80 (-0.03, 0.49)	0.83 (-0.01, 0.52)	0.84 (0.00, 0.53)	0.83 (0.00, 0.53)	0.84 (0.00, 0.53)
MRPC	0.84 (-0.02, 0.15)	0.84 (-0.02, 0.16)	0.86 (0.00, 0.18)	0.86 (0.00, 0.54)	0.87 (0.00, 0.55)
SST-2	0.92 (-0.01, 0.43)	0.92 (0.00, 0.43)	0.93 (0.00, 0.43)	0.92 (0.00, 0.43)	0.92 (0.00, 0.43)
<i>Resnet18</i>					
CIFAR10	0.89 (0.03, 0.67)	0.92 (0.00, 0.78)	0.93 (0.00, 0.83)	0.93 (0.00, 0.83)	0.93 (0.00, 0.83)
CIFAR100	0.73 (0.03, 0.71)	0.75 (0.01, 0.74)	0.76 (0.00, 0.75)	0.76 (0.00, 0.75)	0.76 (0.13, 0.75)
Flowers102	0.84 (0.04, 0.83)	0.84 (0.04, 0.84)	0.89 (0.00, 0.88)	0.89 (0.00, 0.88)	0.89 (0.00, 0.88)
<i>Resnet50</i>					
CIFAR10	0.92 (0.01, 0.81)	0.93 (0.00, 0.83)	0.93 (-0.01, 0.83)	0.94 (-0.01, 0.84)	0.94 (-0.01, 0.84)
CIFAR100	0.69 (0.09, 0.63)	0.76 (0.02, 0.75)	0.78 (0.00, 0.77)	0.78 (0.00, 0.77)	0.78 (0.00, 0.77)
Flowers102	0.76 (0.10, 0.74)	0.82 (0.04, 0.80)	0.86 (0.00, 0.84)	0.86 (0.00, 0.84)	0.85 (0.00, 0.84)
<i>ViT-B_16-224</i>					
CIFAR10	0.99 (0.00, 0.89)	0.99 (0.00, 0.89)	0.99 (0.00, 0.89)	0.99 (0.07, 0.89)	0.93 (-0.02, 0.93)
CIFAR100	0.92 (-0.02, 0.92)	0.93 (-0.02, 0.92)	0.93 (-0.02, 0.92)	0.93 (-0.02, 0.93)	0.93 (-0.02, 0.93)
Flowers102	1.00 (0.00, 0.98)	1.00 (0.00, 0.98)	1.00 (0.00, 0.99)	1.00 (0.00, 0.99)	1.00 (0.00, 1.00)

F Baseline Performance Degradation

F.1 Sparsity-aware lock

We present below the degradation in performance from the transfer of the dense *original* model, i.e. before locking, to a higher-levels of sparsity, p .

Table 11: Results are presented as $Acc_{\text{authorised}}(\Delta_{\text{base}} = Acc_{\text{authorised}} - Acc_{\text{unauthorised}})$

Dataset	Pruning Levels				
	0.05	0.10	0.25	0.50	0.75
<i>BERT</i>					
MRPC	0.86 (0.00)	0.86 (0.00)	0.86 (0.01)	0.86 (0.18)	0.86 (0.54)
SST-2	0.92 (-0.00)	0.92 (-0.00)	0.92 (-0.00)	0.92 (0.03)	0.92 (0.30)
CoLA	0.84 (-0.00)	0.84 (-0.00)	0.84 (0.01)	0.84 (0.53)	0.84 (0.53)
<i>Resnet18</i>					
CIFAR10	0.93 (0.00)	0.93 (0.00)	0.93 (0.00)	0.93 (0.06)	0.93 (0.68)
CIFAR100	0.76 (0.00)	0.76 (-0.00)	0.76 (0.01)	0.76 (0.07)	0.76 (0.08)
Flowers102	0.89 (0.00)	0.89 (0.01)	0.89 (0.01)	0.89 (0.08)	0.89 (0.68)
<i>Resnet50</i>					
CIFAR10	0.93 (-0.00)	0.93 (-0.00)	0.93 (0.00)	0.93 (0.06)	0.93 (0.70)
CIFAR100	0.78 (-0.00)	0.78 (-0.00)	0.78 (0.01)	0.78 (0.07)	0.78 (0.65)
Flowers102	0.86 (0.00)	0.86 (0.00)	0.86 (0.01)	0.86 (0.10)	0.86 (0.66)
<i>ViT-B_16-224</i>					
CIFAR10	0.99 (-0.00)	0.99 (-0.00)	0.99 (0.00)	0.99 (0.07)	0.99 (0.00)
CIFAR100	0.91 (0.00)	0.91 (0.01)	0.91 (0.01)	0.91 (0.30)	0.91 (0.90)
Flowers102	1.00 (0.00)	1.00 (0.00)	1.00 (0.00)	1.00 (0.23)	1.00 (0.98)

As seen from Table 11, in most settings, models can consistently be deployed at a pruning level of up to $p = 0.5$, without incurring a notable cost in terms of accuracy. In certain cases, for example *ResNet18* on CIFAR100 and *ViT-B_16-224* on CIFAR10, even a sparsity level of $p = 0.75$ does not significantly affect performance. Table 11 therefore highlights that the significant degradation in performance seen when deploying locked models on unauthorised levels of sparsity 5 can attributed to sparsity-aware locking, and not merely pruning.

F.2 Quantisation-aware lock

We present below the degradation in performance from the transfer of the *original* model, i.e. before locking, to different arithmetics.

Table 12: Results are presented as $Acc_{\text{authorised}}(\Delta_{\text{base}} = Acc_{\text{authorised}} - Acc_{\text{un-authorized}})$

authorised \rightarrow Unauthorised	Resnet18	Resnet50
FP32 \rightarrow 8-bit MiniFloat	0.88 (0.00)	0.88 (0.01)
Int8 \rightarrow 8-bit MiniFloat	0.88 (0.00)	0.88 (0.01)
16-bit MiniFloat \rightarrow Int8	0.88 (0.00)	0.88 (0.01)
FP16 \rightarrow Int8	0.88 (0.00)	0.88 (-0.01)

There are negligible performance drops, if any, from quantising the base model to an un-authorized arithmetic, as seen by the low Δ_{base} values. Note that this is as the base-model was partially trained with a quantisation-aware loss at **Int8**. Like with sparsity-aware locking, Table 12 clearly shows that the degradation in accuracy when the locked model is transferred to unauthorised arithmetic schemes is a result of soft-locking, and not merely from the differences in model representation across hardware.

F.3 Soft-Locking Optimisation Profiles

F.3.1 Sparsity-aware Lock

We present below the validation curves of the soft-locking optimisation procedure for the three vision models for a subset of the datasets, *CIFAR10*, *CIFAR100*, and pruning proportions, $p = \{0.05, 0.25, 0.50\}$.

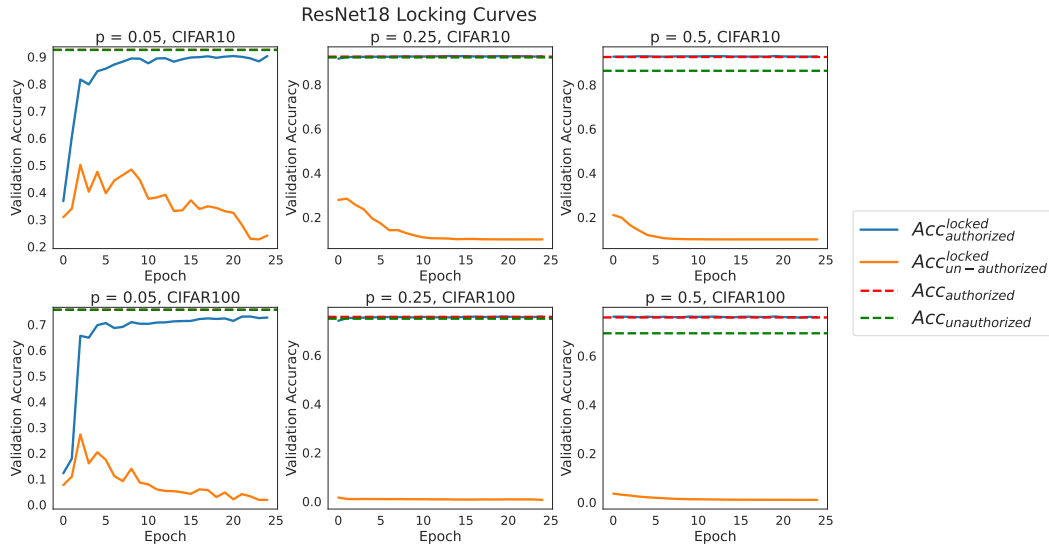


Figure 3: *ResNet18* locking curves

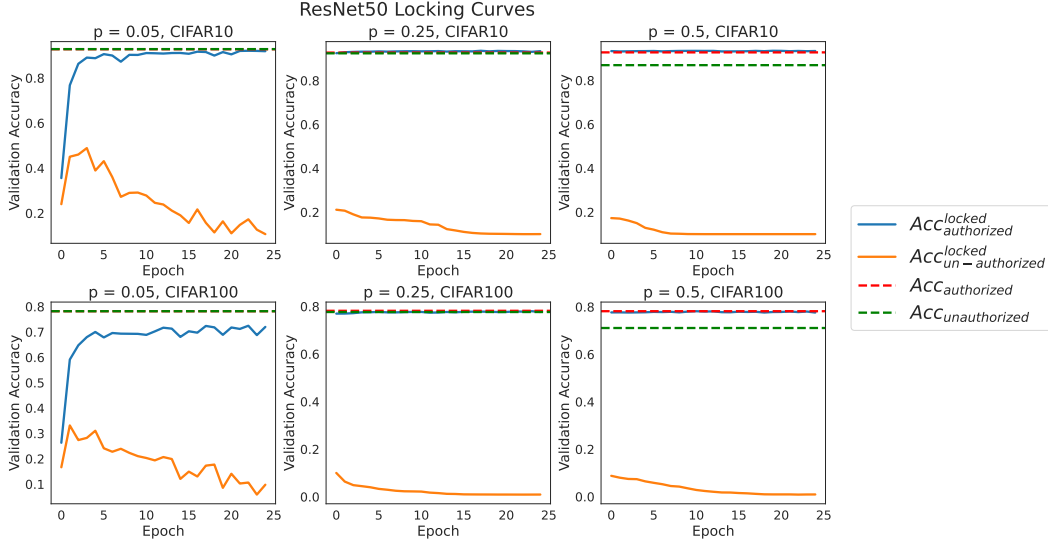


Figure 4: *ResNet50* locking curves

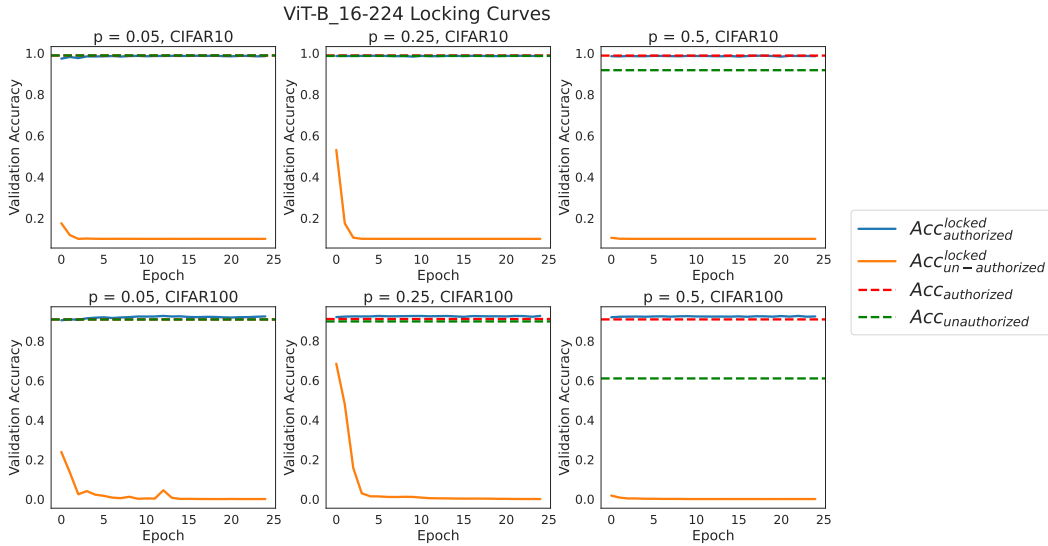


Figure 5: *ViT-B_16-224* locking curves

The optimisation profiles generally converge much more rapidly, across datasets and models, for higher pruning proportions, p . This reinforces the intuitive result that the optimisation solved is *easier* for greater sparsity values, and hence, larger values of p . For $p = 0.05$, the performance of the authorised locked model ($Acc_{authorized}^{locked}$) first reduces in performance, suggesting the optimisation is dominated by the second term of the manipulation loss function. Across the course of the optimisation, this accuracy increases to an acceptable level, due to the eventual effect of the first term of the loss function.

The notable exception to this trend is *ViT-B_16-224*. We posit that this is due to its increased size (in number of parameters), which allows for a decoupling of the opposing optimisation objectives, as the number of parameters at 5% is much greater in *ViT-B_16-224* than in the *ResNet* models. The larger number of parameters can be used to effectively encode the differential knowledge between the authorised and unauthorised variants of the model.

F.4 Quantisation-aware lock

We present below the validation curves of the quantisation-aware locking procedure for the ResNet models on *CIFAR10*, *CIFAR100* - for the authorised, unauthorised arithmetic pairs presented in 6. Note the failure of the locking optimisation procedure for **MiniFloat8** \rightarrow **Int8**.

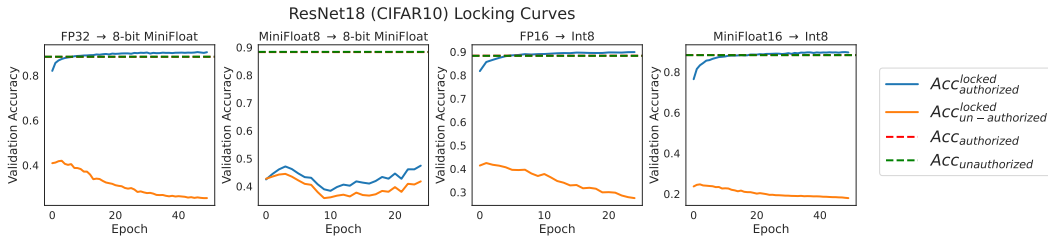


Figure 6: *ResNet18* locking curves

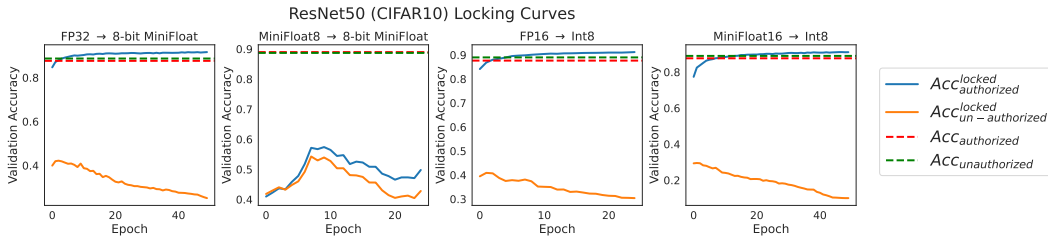


Figure 7: *ResNet50* locking curves

G Appendix

In the following section, we present various miscellaneous findings regarding the sparsity-aware lock.

G.1 Specificity of Sparsity-Aware Locking

We present below the the performance of locked model across a range of sparsity levels for the *ResNet* models on CIFAR10.

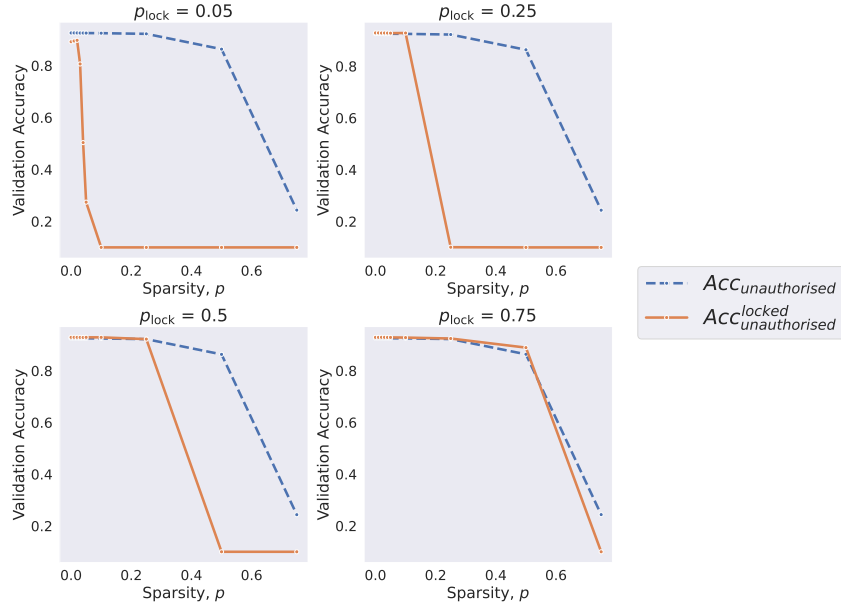


Figure 8: Validation accuracy across sparsity levels (*ResNet18* on *CIFAR10*)

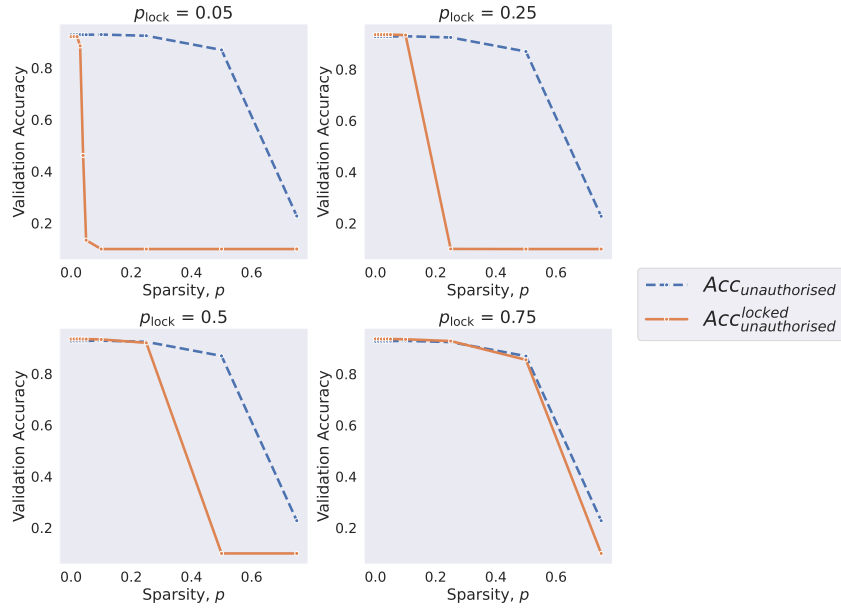


Figure 9: Validation accuracy across sparsity levels (*ResNet50* on *CIFAR10*)

In both models and all locking levels, p_{lock} , there is a highly localised drop in accuracy at the sparsity-level that is locked. This is desirable for setting in which the provider that is locking a proprietary model is aware of the downstream sparsity-level utilised by unauthorised users. If this is not known, or there is no single sparsity level that is unauthorised, models can be conservatively locked at $p_{\text{lock}} = 0.05$. As seen in 8 and 9, locking the model at $p_{\text{lock}} = 0.05$ effectively renders transfer to any level of sparsity that enables efficient execution on hardware useless.

G.2 Attacking soft-locking

If the unauthorised user has access to data, they may *attack* the soft-locking procedures by re-training the models on the unauthorised hardware. For re-training, it is natural for the user to employ a quantisation- or pruning-aware loss and minimise the loss of the quantised or the pruned model.

To investigate the effectiveness of re-training, we re-trained a subset of the locked vision models, namely *Resnet18* and *ResNet50*, on CIFAR100. We present below the re-training curves of the sparsity-locked models.

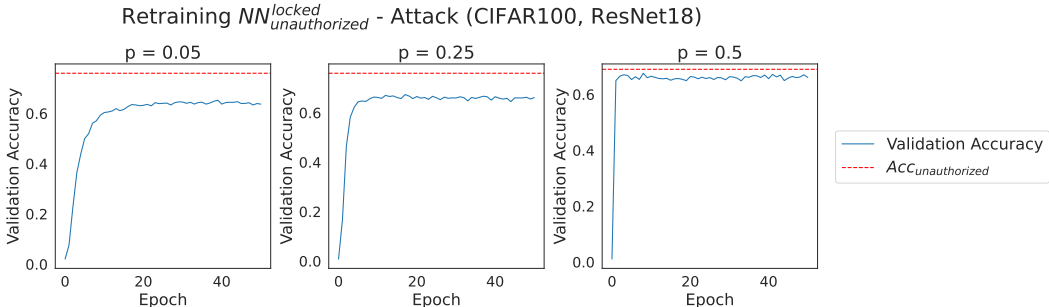


Figure 10: Re-training sparsity-locked *ResNet18* on CIFAR100

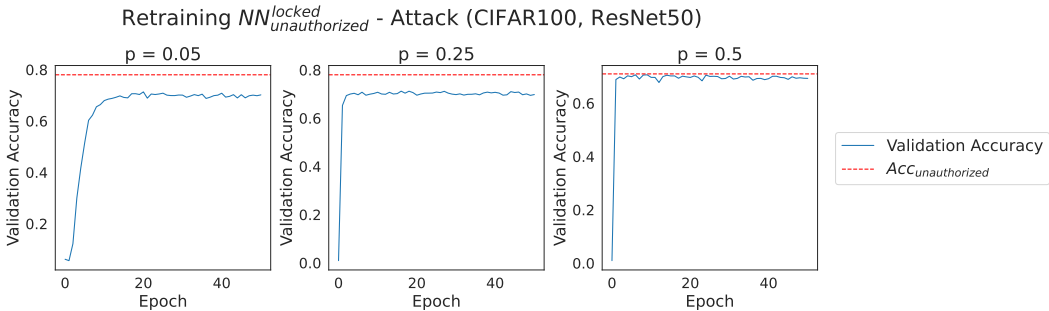


Figure 11: Re-training sparsity-locked *ResNet50* on CIFAR100

In both models, re-training the models locked at $p = 0.05$ and $p = 0.25$ does not return them to the accuracy of the unlocked model deployed on unauthorised hardware. For the models locked at $p = 0.50$, the majority of the accuracy is recovered in roughly 5 epochs.

Below, we also present the training curves resulting from re-training the sparsity-locked *BERT* models on the GLUE tasks, with a pruning-aware loss. The fine-tuning curve of a base *BERT* model, at the same level of sparsity, with a pruning-aware loss is presented as a baseline of reference. The recovery of performance of locked models is comparable to the fine-tuning a sparse *BERT* model from scratch. However, we note that GLUE tasks may not provide the resolution that the previous vision tasks did, as 5 epochs are sufficient for convergence in this setting.

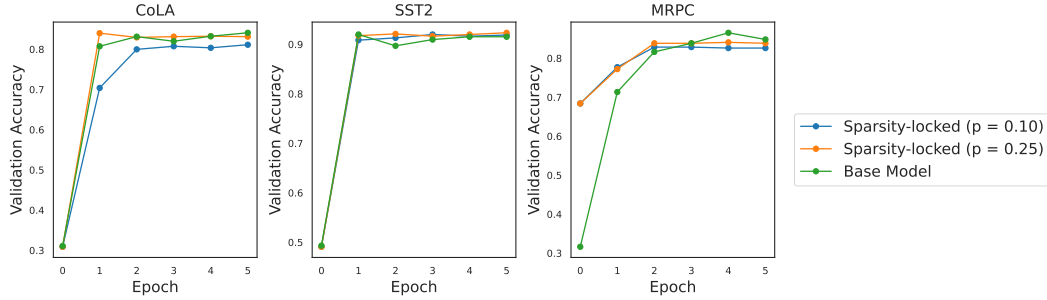


Figure 12: (Re-)Fine-tuning of Sparsity-locked Models

G.3 Effect of Sparsity-Aware Locking on Prune Sum

To better understand the workings of the sparsity-locking scheme we investigated the evolution of the *prune sum*, which is the sum of the absolute values of the weights pruned. For brevity, we present the evolution of prune sum for only *ViT-B_16-224*.

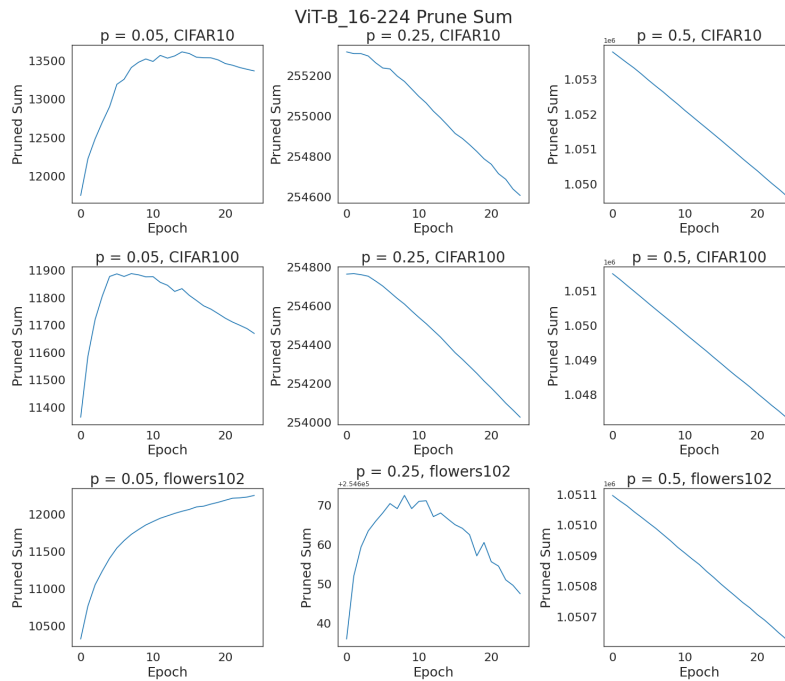


Figure 13: Evolution of Prune Sum during Sparsity-Locking (*ViT-B_16-224*)

Note that the y -axis scales of the different settings are vastly different. Interestingly, this diagnostic illuminates that there are two regimes for the sparsity-aware locking scheme, dependent on the value of p . For locking low-levels of sparsity and p , the locking procedure increases the absolute magnitudes of the p -smallest parameters which, to a first-order, increases their *importance* in model inference. At larger values of p , increases to the prune sum are negligible, if at all, suggesting the locking procedure does not rely on the increasing of magnitudes.

H Parameter transform distributions

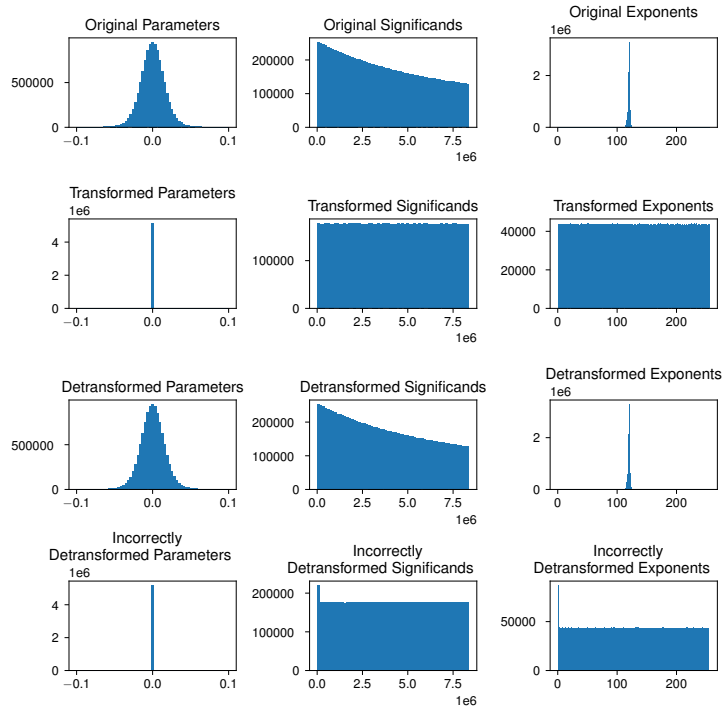


Figure 14: AES encryption transformation method

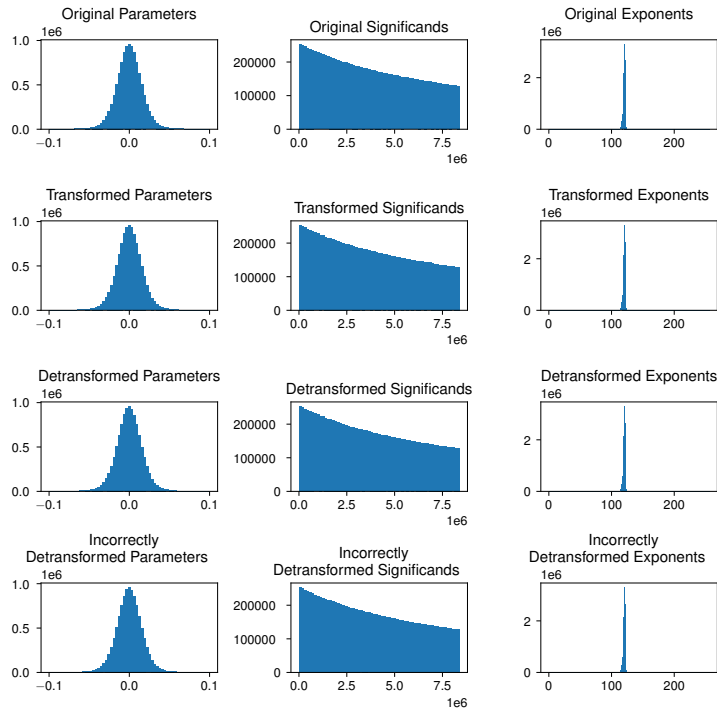


Figure 15: Shuffle transformation method

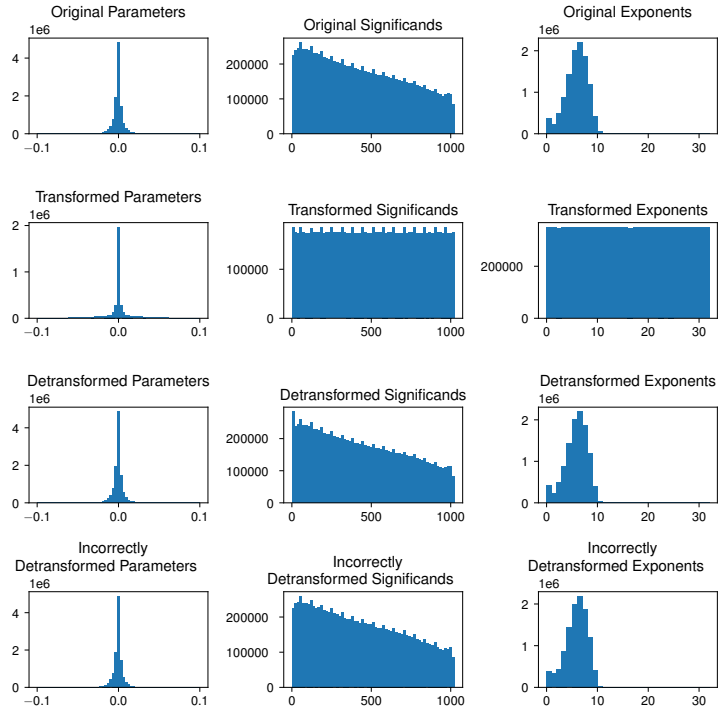


Figure 16: Pretransformed AES encryption transformation method, with direct estimation of distribution, on 16-bit floating point

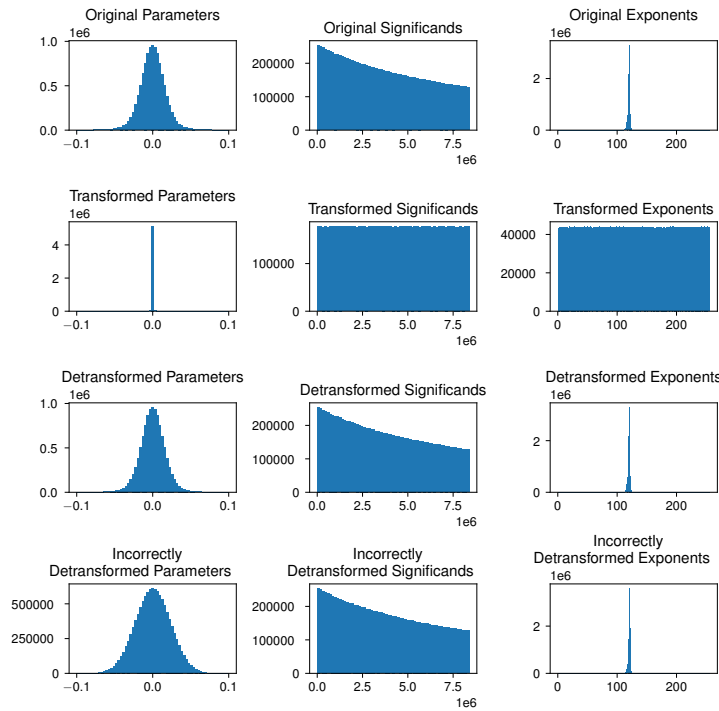


Figure 17: Pretransformed AES encryption transformation method, assuming distribution to be Gaussian, on 32-bit floating point

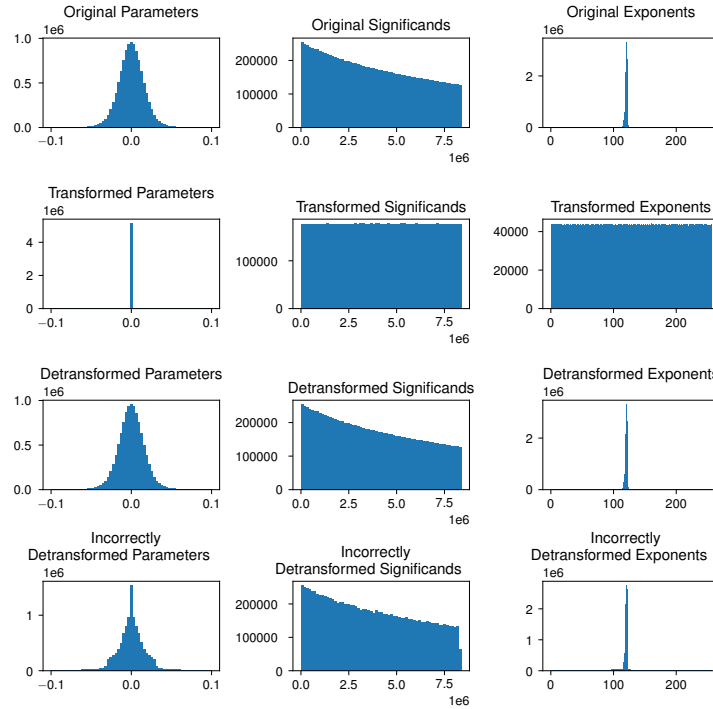


Figure 18: Pretransformed AES encryption transformation method, directly estimating distribution but assuming significant and exponent to be independent, on 32-bit floating point

I Finite Precision Fingerprints

Table 13: Finite precision fingerprint on various devices

Device	Fingerprint
GTX 1080Ti	834a709ba2534ebe3ee1397fd4f7bd288b2acc1d20a08d6c862dcd99b6f04400
RTX 2080Ti	157c46f3245781907678d796984d27f21b3828d434c770ed85f7ac03bf11fe9f
RTX 3090	e2b643bf633651bd14296a6205d7ef7e7e0dbb8c837d492e56695e3999eae638
RTX A6000	68085f05ecc499655bf7923c8a7f65a2a05e72ec67dfc1fb342377a04163c78f
RTX A6000 (<i>runpod.io</i>)	5bc85507944291de0716edaa3e77c6bf56d2fa173c1d207089d3db089638e83

J CUDA code to produce clock fingerprint

```

1 /* Copyright (c) 2024, Eleanor Clifford
2 * Copyright (c) 2022, NVIDIA CORPORATION. All rights reserved.
3 *
4 * Redistribution and use in source and binary forms, with or without
5 * modification, are permitted provided that the following conditions
6 * are met:
7 *   * Redistributions of source code must retain the above copyright
8 *     notice, this list of conditions and the following disclaimer.
9 *   * Redistributions in binary form must reproduce the above
10 *     copyright notice, this list of conditions and the following
11 *     disclaimer in the documentation and/or other materials
12 *     provided with the distribution.
13 *   * Neither the name of NVIDIA CORPORATION nor the names of its
14 *     contributors may be used to endorse or promote products
15 *     derived from this software without specific prior written
16 *     permission.

```



```

17 *
18 * THIS SOFTWARE IS PROVIDED BY THE COPYRIGHT HOLDERS ‘‘AS IS’’ AND
19 * ANY EXPRESS OR IMPLIED WARRANTIES, INCLUDING, BUT NOT LIMITED TO,
20 * THE IMPLIED WARRANTIES OF MERCHANTABILITY AND FITNESS FOR A
21 * PARTICULAR PURPOSE ARE DISCLAIMED. IN NO EVENT SHALL THE
22 * COPYRIGHT OWNER OR CONTRIBUTORS BE LIABLE FOR ANY DIRECT, INDIRECT,
23 * INCIDENTAL, SPECIAL, EXEMPLARY, OR CONSEQUENTIAL DAMAGES
24 * (INCLUDING, BUT NOT LIMITED TO, PROCUREMENT OF SUBSTITUTE GOODS OR
25 * SERVICES; LOSS OF USE, DATA, OR PROFITS; OR BUSINESS INTERRUPTION)
26 * HOWEVER CAUSED AND ON ANY THEORY OF LIABILITY, WHETHER IN CONTRACT,
27 * STRICT LIABILITY, OR TORT (INCLUDING NEGLIGENCE OR OTHERWISE)
28 * ARISING IN ANY WAY OUT OF THE USE OF THIS SOFTWARE, EVEN IF ADVISED
29 * OF THE POSSIBILITY OF SUCH DAMAGE.
30 */
31
32 // System includes
33 #include <assert.h>
34 #include <stdint.h>
35 #include <stdio.h>
36 #include <ieee754.h>
37 #include <limits.h>
38
39 // CUDA runtime
40 #include <cuda_runtime.h>
41
42 // helper functions and utilities to work with CUDA
43 #include <helper_cuda.h>
44 #include <helper_functions.h>
45
46 #define INNER_LOOP 512
47 #define NUM_BLOCKS 128
48 #define NUM_THREADS 8
49 #define NUM_TRIES 16
50
51 // This kernel does something which doesn't matter.
52 // The timing results are stored in device memory.
53 __global__ static void timedFunction(
54     const float *input, float *output,
55     clock_t *timer
56 ) {
57     extern __shared__ float shared[];
58
59     const int tid = threadIdx.x;
60     const int bid = blockIdx.x;
61
62     // Copy input.
63     shared[tid] = input[tid];
64     shared[tid + blockDim.x] = input[tid + blockDim.x];
65
66     if (tid == 0) timer[bid] = clock();
67
68     // Do some stuff
69     for (size_t i = 0; i < INNER_LOOP; i++) {
70         for (int d = blockDim.x; d > 0; d /= 2) {
71             __syncthreads();
72
73             if (tid < d) {
74                 float f0 = shared[tid];
75                 float f1 = shared[tid + d];
76
77                 if (f1 < f0) {
78                     shared[tid] = (f0 + f1);
79                 }
80             }
81         }
82     }

```

```

82     }
83
84     // Write result.
85     if (tid == 0) output[bid] = shared[0];
86     __syncthreads();
87     if (tid == 0) timer[bid + gridDim.x] = clock();
88
89 }
90
91 // Start the main CUDA Sample here
92 int main(int argc, char **argv) {
93     cudaSetDevice(2);
94
95     float *dinput = NULL;
96     float *doutput = NULL;
97     clock_t *dtimer = NULL;
98
99     clock_t timer[NUM_BLOCKS * 2];
100    float input[NUM_THREADS * 2];
101
102    for (int i = 0; i < NUM_THREADS * 2; i++) {
103        input[i] = (float)i;
104    }
105
106    long fastestClock = LONG_MAX;
107    for (int j = 0; j < NUM_TRIES; j++) {
108
109        checkCudaErrors(
110            cudaMalloc((void **)&dinput, sizeof(float) * NUM_THREADS * 2)
111        );
112        checkCudaErrors(
113            cudaMalloc((void **)&doutput, sizeof(float) * NUM_BLOCKS)
114        );
115        checkCudaErrors(
116            cudaMalloc((void **)&dtimer, sizeof(clock_t) * NUM_BLOCKS * 2)
117        );
118
119        checkCudaErrors(
120            cudaMemcpy(dinput, input, sizeof(float) * NUM_THREADS * 2,
121                    cudaMemcpyHostToDevice)
122        );
123
124        timedFunction<<<
125            NUM_BLOCKS, NUM_THREADS, sizeof(float) * 2 * NUM_THREADS
126        >>>(dinput, doutput, dtimer);
127
128        checkCudaErrors(
129            cudaMemcpy(timer, dtimer, sizeof(clock_t) * NUM_BLOCKS * 2,
130                    cudaMemcpyDeviceToHost)
131        );
132
133        checkCudaErrors(cudaFree(dinput));
134        checkCudaErrors(cudaFree(doutput));
135        checkCudaErrors(cudaFree(dtimer));
136
137        for (int i = 0; i < NUM_BLOCKS; i++) {
138            long t = (timer[i + NUM_BLOCKS] - timer[i]);
139            if (t < fastestClock) {
140                fastestClock = t;
141            }
142        }
143    }
144
145    printf("%x\n", (unsigned int)fastestClock);
146

```

```
147     return EXIT_SUCCESS;
148 }
```

K Python code to produce finite precision fingerprint

```
1 import torch
2 import hashlib
3 import numpy as np
4
5 dev = "cuda"
6
7 torch.manual_seed(0)
8 inp = torch.randn(1, 50, 50, 100)
9 m = torch.nn.Sequential(
10     torch.nn.Linear(100, 1000),
11     torch.nn.Linear(1000, 10000),
12     torch.nn.Linear(10000, 10),
13 )
14
15 m = m.to(dev)
16 inp = inp.to(dev)
17
18 out = []
19
20 orig = None
21 with torch.no_grad():
22     for i in range(1, 10):
23         _input = torch.cat(i * [inp]).clone()
24         output = m(_input)
25
26         if orig is None:
27             orig = output[0].clone().detach()
28
29         out.append(float((orig - output).sum()))
30
31 print(hashlib.sha256(np.array(out)).hexdigest())
```

L Experiment Compute Resources

The soft locking experiments consume most of the compute resources. We conducted all sparsity-aware locking and quantisation-aware locking on NVIDIA V100 GPUs and 18-core Intel Xeon (Broadwell) processors. The fine-tuning took around 1 GPU hours per trial on average, and in total, the fine-tuning time was around 180 GPU hours. We spent additional time on preliminary and failed experiments, which is around 40 GPU hours in total. The emulation cost experiments were performed on three NVIDIA RTX A6000 GPUs with an AMD EPYC 7713 64-core processor. The emulation cost experiments took around 4 GPU hours. The hard locking experiments were conducted on NVIDIA GTX 1080Ti, RTX 2080Ti, RTX 3090, RTX A6000 GPUs, and took 10 GPU hours in total.